2. Exploiting wetting phenomena to tailor 1D nano- and microstructures

2.1 Wetting on a macroscopic scale

As a large part of the work in this thesis deals with wetting of porous materials, the phenomena involved in wetting are first discussed in this chapter. It entails a detailed discussion of the underlying physics even though a lot of open questions will remain unanswered.

2.1.1 Contact angle and Young's law

In the theory of classical capillarity of wetting phenomena, the interfacial tension γ_{ij} plays a key role. It represents the free energy necessary to increase by one unit the area of contact between two different phases i and j. The origin of this free energy can be understood physically as follows: Inside a dense phase, i, the molecules attract each other, and they can interact better with neighbors of the same species i when located in the bulk material than when located close to the interface to another phase j.

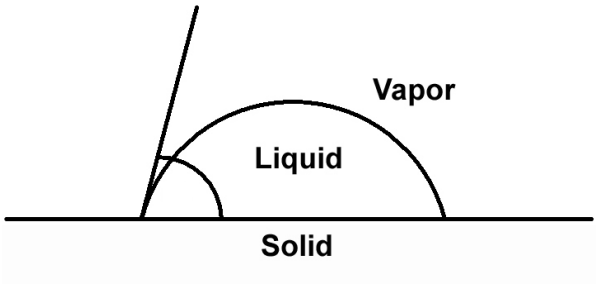

Figure 2.1: Schematic of wetting during the coexistence of three phases, respectively liquid, solid and vapor phases. The contact angle is denoted by θ.

Suppose we have a solid substrate S wetted by a liquid L in contact with a vapor V, as shown in figure 2.1. Three interfaces can then be distinguished: liquid-vapor, solid-liquid, and solid-vapor with the correspondingly associated free surface energies: γ_{LV}, γ_{SL} and γ_{SV}, respectively. In figure 2.1, a tendency is shown towards wetting rather than dewetting. Indeed, out of the two phases, liquid and vapor, the solid substrate prefers the liquid and disfavors the vapor. This can be seen from the spreading of the liquid on the solid substrate: the contact angle θ is less than $90°$. Experimentally, the contact angle must be measured close enough to the wall, that is, within a few percent of the capillary length a_0 [56]. This length is a measure of the distance over which the liquid-vapor interface is curved, and results from the competition of surface tension and gravity. It is defined as [56]:

$$a_0 = \sqrt{\frac{2\gamma_{LV}}{g\Delta\rho}} \tag{2.1}$$

where g is the gravitational acceleration and $\Delta\rho$ is the density difference of liquid and vapor. Typical values of a_0 are of the order of one millimeter. Another point needs to be noted is that all the free energies are "far-field", which means that these interfacial free energies act "sufficiently" far way from the region near the contact line of molecular dimensions.

In figure 2.1, it can also be figured out that, although the inequality $\gamma_{LS} < \gamma_{SV}$ applies, a direct solid-vapor contact is still tolerated. However, when the preference for adsorption of the liquid would be further increased (for example, by changing the temperature), the vapor may become excluded from contact with the solid. Then, a liquid layer will intrude between solid and vapor. This is termed *complete wetting*, whereas the situation in figure 2.1 represents *partial wetting*. The thickness of the liquid wetting layer in the case of complete wetting is typically a few hundred $\mathring{A}$, as will be discussed in more details in section 2.2.2. The equilibrium surface free energy of the solid-vapor interface is consequently defined as

$$\gamma_{SV} \geq \gamma_{SL} + \gamma_{LV} \tag{2.2}$$

at complete wetting.

For partial wetting, on the other hand, the inequality applies:

$$\gamma_{SV} < \gamma_{SL} + \gamma_{LV} \tag{2.3}$$

which expresses that although a solid-liquid contact is preferred, a solid-vapor interface has lower free energy than the combination of solid-liquid and liquid-vapor interfaces. Balancing the components of these forces along the direction parallel to the substrate and perpendicular to the contact line (the vertical direction in figure 2.1) leads to [57]:

$$\cos\theta = \frac{\gamma_{SV} - \gamma_{SL}}{\gamma_{LV}} \tag{2.4}$$

The angle θ is the contact angle, as defined in figure 2.1. The equation 2.4 is also known as Young's law. Note that the equation 2.4 can also serve as the thermodynamic definition of the contact angle, when the surface free energies are known, but no direct observation of θ is made. Clearly, complete wetting corresponds to θ = 0. Young's law needs to be generalized as soon as the surface tension of the interface between the two adsorbed phases is anisotropic. In the case of partial wetting, Young's law expresses the mechanical equilibrium of the forces (per unit length) that the interfaces exert on the contact line along which they meet.

The contact angle given by Young's equation is static, i.e., Young's law applies to the equilibrium state of the system. However, if the three phase (liquid/solid/vapor) boundary is in actual motion, the angles produced are called *dynamic contact angles* and are referred to as "advancing" and "receding" angles, as shown in figure 2.2. The difference between "advanced" and "advancing", "receded" and "receding" is that in the static case motion is incipient while in the dynamic case motion is actual. During its motion toward an equilibrium state, a liquid drop scans a range of dynamic contact angles. Dynamic contact angles may be determined at various rates of speed. Dynamic contact angles measured at low velocities should be equal to properly measured static angles.

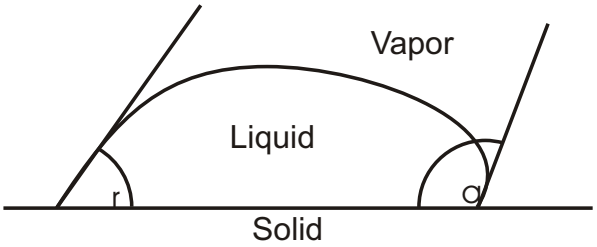

Figure 2.2: Side view of a sessile water drop on a solid surface showing advancing and receding contact angles (θ_a and θ_r).

2.1.2 Tanner's law

It is important to notice that the effect of body forces such as gravity on the contact line is vanishingly small and that, therefore, equation 2.4 is valid even in the presence of gravity or any other body force. Only such forces as viscous forces which might become increasingly large at the contact line can affect Young's law. In the case when the surface tension is the only driving force, Tanner's spreading law [58] is an approximated solution of the hydrodynamics of spreading.

Regard a nonvolatile liquid drop on a nonreactive smooth surface when inertial or viscoelastic effects are neglected. Furthermore, the drops are supposed to be small enough for the gravity to be negligible.

On a macroscopic scale, according to Tanner, a universal spreading equation, regarded as Tanner's law, reads [58]:

$$\frac{da}{dt} = v^* \theta^3 \tag{2.5}$$

where a is the radius of the liquid-substrate contact area and v^* a characteristic velocity, defined by

$$v^* = \frac{\gamma_{LV}}{\mu} \tag{2.6}$$

where μ is the viscosity of the spreading liquid.

As a result of equation 2.5, this model gives the radius a as a function of the time t in the complete wetting regime as $a \propto t^n$.

Tanner's law has also been obtained by de Gennes [57] from a balance between the viscous dissipation and the work done by the surface tension force. He uses a general equation that describes the profile of the droplet near the edge when the long-range forces are negligible. In this more general theory, the dependence of a on the droplet volume Ω is obtained by:

$$a \propto \Omega^m (v^* t)^n \tag{2.7}$$

with $n = 0.1$, $m = 0.3$.

Lopez *et al.* [59] have analyzed the situation, when gravity is the main driving force. They obtained a similar power law with $n = 0.125$ and $m = 0.375$. These theories are based on steady state arguments focusing on the edge of the film and using a lubrication approximation. Tanner [58] and Lopez [59] compared theories to experiments, finding good agreement in both cases. Hydrodynamic models, however, do not predict the dependence of n on a change such

as in temperature or in pH value which alter both the surface tension and the viscosity. The lack of a controlled experimental environment might therefore explain the range of observed values of n and m.

2.1.3 Spreading coefficient

If non-equilibrium situations are dealt with, we may have a solid/vapor interfacial tension γ_{SV} that is larger than $\gamma_{SL} + \gamma_{LV}$. The difference

$$S = \gamma_{SV} - \gamma_{SL} - \gamma_{LV} \tag{2.8}$$

is called the spreading coefficient.

The transition from partial to complete wetting can be discussed in terms of the equilibrium spreading coefficient S as follows. When S is positive, the spreading is energetically favored. The liquid spontaneously spreads and tends to cover the whole solid surface. Using Young's law (equation 2.4), we obtain:

$$S = \gamma_{LV}(\cos\theta - 1) \tag{2.9}$$

so that for partial wetting $S < 0$, and for complete wetting $S = 0$. The wetting kinetics can now be characterized by the way in which S tends to zero, or, equivalently, the way in which $\cos\theta$ tends to 1.

Up to now, all the situations aforementioned can be summarized in terms of contact angle as:

- complete wetting $\leftrightarrow \theta = 0$
- partial wetting $\leftrightarrow 0 < \theta < 90\,^\circ$
- partial drying $\leftrightarrow 90\,^\circ < \theta < 180\,^\circ$

From the values of bulk cohesive energy, there are two main types of solids: (a) hard solids (covalent, ionic, or metallic), which have a solid/vapor interfacial energy of γ_{SV} - 500 to 5000 ergs/cm^2 and (b) weak molecule crystals and organic liquids (bound by van der Waals forces, or in some special cases, by hydrogen bonds), which have a γ_{SV} - 50 ergs/cm^2 [60]. Most molecular liquids can have complete wetting on high-energy surfaces. This can be explained qualitatively as follows: The underlying solid usually has a polarity much higher than that of the liquid. In contrast, low-energy surfaces can also give rise to a partial or complete wetting. It depends on the surface tension of the liquid. For a complete wetting, there exists a "critical surface tension". Only when the surface tension of a chosen liquid is smaller than the critical value can a complete wetting happen.

2.2 Wetting on a microscopic scale

2.2.1 Role of the disjoining pressure

As mentioned earlier, if the spreading coefficient S is positive, spontaneous spreading occurs, and the equilibrium situation corresponds to a complete coverage of the solid by a thin liquid film. However, several measurements of the spreading kinetics of liquids on a large variety of

substrates seem to give spreading kinetics approximately independent of S, and the adequacy of a description based on interfacial energies and simple hydrodynamic concepts has been widely debated [61]. To solve this dilemma, Joanny and de Gennes pointed out the role of molecular long-range forces, which may result in the formation of a precursor film [57, 62]. They stated that when a film is very thin, long-range forces cannot be neglected. These forces may be electrostatic, steric, or van der Waals in nature. In this thesis, all the long-range forces are restricted to van der Waals interactions, which always exist between two atoms or molecules. The potential of interaction is attractive and decreases with intermolecular distance r as r^{-6}; this is the so-called nonretarded regime. When this potential is integrated over all pairwise interactions between two half-spaces separated by a small distance e, one finds a slow decreasing potential[1] [63]:

$$W(e) = -\frac{A}{12\pi e^2} \tag{2.10}$$

where A is an effective Hamaker constant [64] which contains all non-geometric contributions to interaction, on the order of a few k_bT (where k_b is the Boltzmann constant and T is the absolute temperature), and e is the liquid film thickness. If A is positive, the interaction is attractive. As an example, A is always positive between two identical bodies, which explains why particles in solution generally flocculate.

In the case of a liquid film deposited on a solid surface, the two half-spaces are different (solid and gas, as shown in figure 2.3), and the Hamaker constant can be either positive or negative. In wetting conditions, A is negative: solid and gas repel each other through the liquid. The effect of long-range forces, that is, the disjoining pressure, Π, is then to make the liquid film thicker, since $W(e)$ has a minimum for an infinite liquid thickness ($e = \infty$). The sign of A can be determined from approximate combining relations [64]:

$$A \simeq A_{SV} + A_{LL} - A_{LV} - A_{SL} \tag{2.11}$$

where the A_{IJ} is Hamaker constant in general between media I and J (which could be either a liquid, vapor or solid), which is proportional to the product of the densities of phases I and J and to the product of their polarizabilities $\alpha_I\alpha_J$. Because the density of the gaseous phase is generally negligible, A is negative when the polarity of the solid is larger than that of the liquid. Therefore, a solid of high surface energy, such as metal or clean glass, should be wet by all the usual liquids.

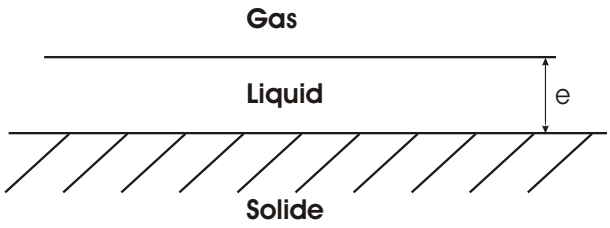

Figure 2.3: Wetting film on a planar solid surrounded by a gas.

2.2.2 Precursor films

For a complete wetting, precursor films may occur. They emanate from a macroscopic droplet and have a thickness e of a few tens of nm in the vicinity of the droplet, and a thickness

[1] For thicker films ($e > 300\mathring{A}$), retarded effects must be considered and $W(e)$ decreases as e^{-3}.

smaller than a molecular monolayer at the microscopic spreading front. As shown in figure 2.4, the precursor film precedes the macroscopic spreading front all around the droplets, with a structure strongly dependent on the spreading coefficient S. If the wetting liquid is non-volatile ("dry spreading"), the only efficient transport of the liquid is by diffusion within the liquid. The precursor film, as depicted in figure 2.4a, forms when the intermolecular forces of attraction between the solid and liquid are sufficiently strong to create positive spreading coefficients and disjoining pressures. As it spreads, more and more material is drawn out of the macroscopic drop into the precursor film, as depicted in figure 2.4b. The submicroscopic structure and dynamics of precursor films depend on the spreading coefficient S and are affected by the local inhomogeneities in surface energy. In this microscopically almost flat precursor film, in which Laplace pressure is negligible, the thickness is governed by long-range forces and decreases towards the equilibrium state which might be either a pancake [57, 62] or a surface gas [65]. In case of pancake, the equilibrium thickness is $e \sim S^{-1/2}$ while in case of a surface gas, the thickness corresponds to a sub-monolayer because of a non-complete surface gas coverage.

As stated by de Gennes [57] and Joanny [62], long-range forces, for example, van der Waals forces, should be taken into account in the spreading phenomenon of precursor film. It is found that, at sufficiently short time, when the macroscopic droplet still acts as a reservoir, the behavior of the precursor film is diffusive and the radial extension (l) on macroscopic scale follows a universal time dependence (t) of the form:

$$l^2 = Dt \tag{2.12}$$

where D is the diffusion coefficient of the liquid within the precursor film. It is different from the conventional diffusion coefficient describing the random motion of particles in the bulk liquid phase or on solid substrates. As a matter of fact, D also depends on the driving forces which cause the film spreading.

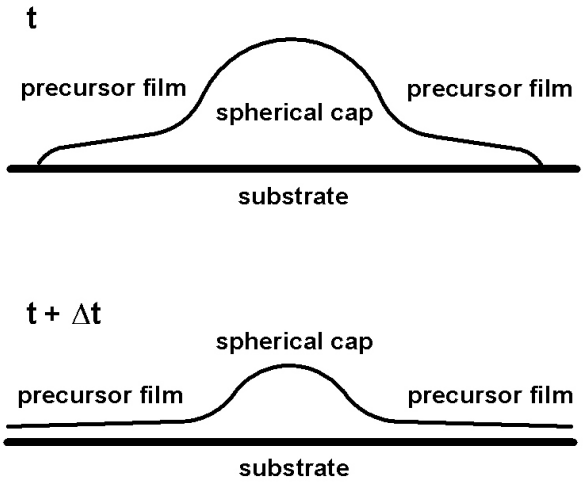

Figure 2.4: Formation of a precursor film during the wetting process of a polymer melt or liquid at time t and $t + \Delta t$.

In a microscopic drop, van der Waals forces are dominant. The following spreading equation stands for van der Waals driven spreading [66]:

$$R(t) = R_0 + v_r t \tag{2.13}$$

with $v_r = \frac{A}{2\mu a_c^k}$. A is an effective Hamaker constant with $A = \frac{B}{12\pi}$ and $k = 2$ for nonretarded van der Waals forces and $A = \frac{C}{9}$ and $k = 3$ for the retarded case, where B and C

are positive constants. a_c is a cutoff length for small values of h (which is the height of the geometrically spherical drop). The supposition that the drop is self-similar and has a spherical profile is justified for the case of the macroscopic drop, where droplet spreading is driven by the Laplace pressure. However, for van der Waals driven spreading, this is only an approximation. In particular near the contact line, it is known that van der Waals pressures deform the drop. Therefore, a_c is not a molecular length scale, but has a much larger value.

It was predicted that the final state of spreading should be a limited flat wetted spot with abrupt edges: a "pancake" [57, 62]. But in the case $S/\gamma_{LV} \geq 1$, the predicted pancake thickness falls in the range of molecular thicknesses: below $20\mathring{A}$. One can expect the details of the structure to be strongly dependent on the *short-range forces*. One should stress also that *molecular diffusion*, which was not taken into consideration in de Gennes' theory, is expected to ultimately destroy the pancake structure if it overcomes the film cohesion [67]. As a matter of fact, when diffusion takes over liquid cohesion, a droplet evolves by diffusion to reach a surface gas [65].

2.3 Wetting by liquid polymers

A polymer is a macromolecule composed of many repeating units of segments. The molecular weight M_0 of a monomer unit is typically between $50\ g/mol$ and $100\ g/mol$, while the total molecular weight $M = nM_0$ can range from 1000 to above 10^6. When in solution or molten, a polymer chain can adopt a number of configurations depending on the net segment-segment forces in the liquid. If these are weak, the polymer assumes the shape of an "unperturbed" random coil. An important length scale is the root mean square radius of the polymer coil. For an unperturbed coil, this is known as the *unperturbed radius of gyration* R_g [68], and is given by

$$R_g = \frac{l_e\sqrt{n}}{\sqrt{6}} = \frac{l_e\sqrt{\frac{M}{M_0}}}{\sqrt{6}} \tag{2.14}$$

where n is the number of segments and l_e the effective segment length. As an example, if $l_e = 1.0\ nm$ and the segment molecular weight is $M_0 = 200$, then for a polymer of $M = 10^6$, R_g has a value of about $29\ nm$. However, the real volume of the chain is only a small fraction of the volume encompassed by R_g. Thus, if the segment width is about the same as the segment length l_e, the molecular volume is $\pi(l_e/2)^2 n l_e \sim n l_e^3$, while the volume encompassed by R_g is $\frac{4}{3}\pi R_g^3 \sim 0.3 n^{\frac{3}{2}} l_e^3$. The ratio of these volumes is $\sim \sqrt{\frac{n}{10}}$. Thus, for a polymer with $n = 1000$ segments, only about $1\ \%$ of the random coil volume is actually occupied.

According to sections 2.1 and 2.2, as nearly all liquids other than liquid metals have free surface energies of less than $75\ ergs/cm^2$ at ordinary temperature. They are allowed to spread spontaneously on "high energy surfaces" such as in organic oxides, silica and most metals. In the case of complete wetting, a sub-micrometer range "precursor film" of liquid spreads ahead of the macroscopically observable liquid edge. The spreading of polymers, which are low energy liquids with large dimension, was first investigated by Ausserré [69]. According to the precursor film profiles of spreading liquid drops studied by Léger *et al.* [70], the thickness profile of a polymeric precursor film decreases as the distance to the macroscopic droplet increases. In its vicinity, the thickness of the precursor film e has a mescoscopic value while at the microscopic spreading front it is below a molecular monolayer. At the microscopic spreading front, the thickness is smaller than the radius of gyration. As a result, individual molecular chains

move by surface diffusion in disentangled states. Glick *et al.* have observed the spreading of polystyrene drops on gold at elevated temperatures and have shown the spreading behavior to be qualitatively consistent with a theoretical picture where the drop acts as a reservoir for a spreading precursor film [71].

2.4 Wetting the walls of cylindrical pores by non-volatile liquids

2.4.1 Capillary rise

The motion of wetting liquid films in cylindrical pores is an important topic in this thesis. When placed inside a cylindrical pore of radius b, whether a liquid plug will spread or not depends on the spreading parameter S, as defined in equation 2.8. The energy (per unit volume) of the spreading liquid is [72]:

$$F_f = \frac{2\pi L(b(\gamma_{SL} - \gamma_{SV}) + (b-e)\gamma_{LV} + bP(e))}{\pi L(2eb - e^2)} \tag{2.15}$$

with $P(e)$ the long-range van der Waals interaction term ($P(e) = \frac{\gamma a^2}{2e^2}$ where $a^2 = \frac{A_{SL} - A_{LL}}{6\pi\gamma}$, A_{SL} and A_{LL} being the Hamaker constants related to solid-liquid and liquid-liquid interactions), while the energy of the unspread drop is

$$F_g = \frac{2\pi bl(\gamma_{SL} - \gamma_{SV})}{\pi b^2 l} = -\frac{2(S + \gamma_{LV})}{b} \tag{2.16}$$

At the drop-film transition, $F_f = F_g$ together with $\frac{\partial F_f}{\partial e} = 0$ gives:

$$S_c = \frac{3}{2}\gamma_{LV}\frac{a}{b}^{2/3} \text{ and } e_c = a^{2/3}b^{1/3} \tag{2.17}$$

- When $S < S_c$, the drop will not spread (situation depicted in figure 2.5b) and partially wets the tube wall, forming an angle of contact (which can be equal to zero, unlike the contact angle of a drop on a planar surface).
- When $S > S_c$, the drop will spread and cover the interior of the pore, making a film (situation depicted in figure 2.5a) of thickness $e = a\sqrt{\frac{3\gamma}{2S}}$. The thickness results from a competition between spreading (expressed by S) and thickening long-range molecular forces (expressed by A) and usually has a value of molecular thickness. This thickness is so small that, even for tiny quantity of liquid, the film will usually coexist with a drop: the pressures of the drop and the film should be the same and this leads to a film thickness of e_c, i.e., the value at the threshold.

2.4.2 The pinch-off mechanism

In his article [73] on the experimental results of the infiltration of disordered glass capillary models consisting of channels with diameters of the order of $100\ \mu m$ with water, Bernadiner described the so-called pinch-off mechanism, which leads to the filling of a capillary with a liquid.

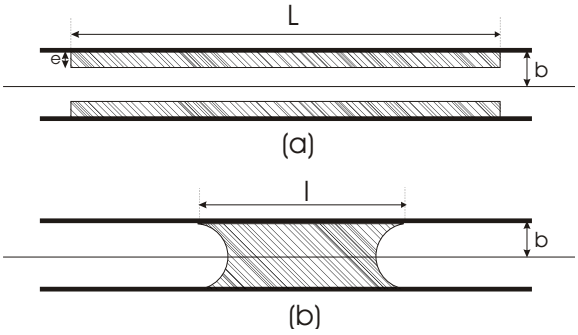

Figure 2.5: Side-view of a capillary tube wetted by a droplet of liquid: (a) a film of thickness e and length L is formed; (b) a drop of length l is formed.

The detailed analysis shows that the pinch-off mechanism consists of four consecutive steps, as shown in figure 2.6: "film flow", "occurrence of instability", "snap-off", and "interface movement", consecutively. Initially, water invades the individual capillary in the form of a thin film moving along the capillary channel surface. This film divides the cross section area of the capillary channel into two layers, water and air. The increase in the thickness of the water layer caused by inflowing water results in the formation of a neck at the air/water interface. Ultimately, the neck snaps, forming two air/water interfaces across the capillary channel. As water continues to flow in the capillary channel, the capillary channel fills up with water, and the interfaces travel in opposite directions along the capillary channel and eventually invade the adjacent pores, forming stagnant boundaries of residual air.

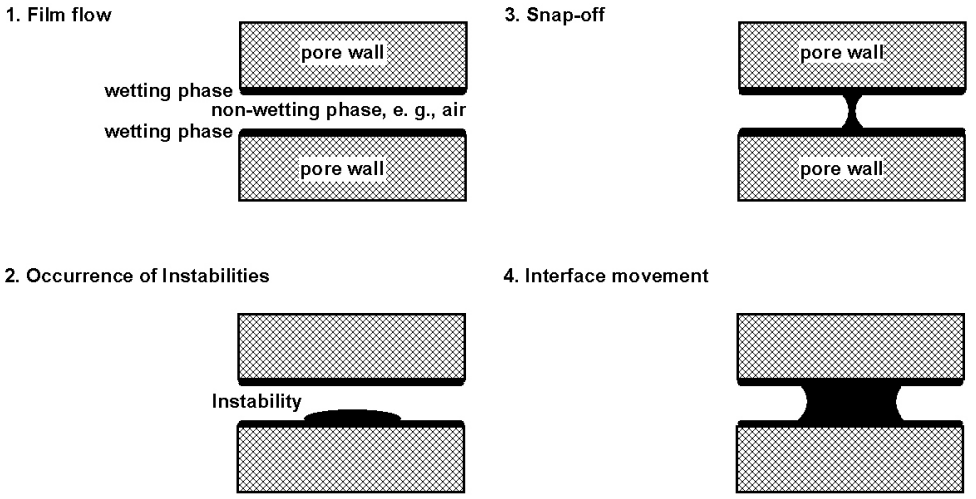

Figure 2.6: The pinch-off mechanism for the formation of the internal front microstructure in capillary with four consecutive stages: (a) film flow; (b) occurrence of instability; (c) snap-off and (d) interface movement.

2.4.3 Rayleigh instability

Joseph Plateau (1801-1883), a Belgian physicist also known for his work on soap films, was the first to study the instability of cylindrical films [74]. Plateau understood that the instability of these films is driven by the liquid surface tension. When the free surface of a liquid cylinder undulates with a wavelength λ, its area decreases [75], provided that λ is larger than the circumference of the cylinder ($2\pi R$ for a liquid jet of radius R, or $2\pi b$ for a film of thickness e on a fiber of radius b for $e << b$). Although the observed longitudinal curvature of the film should oppose the growth of the instability, the curvature associated with the cross-sectional

area of the column, which is larger than the longitudinal curvature, actually governs the growth of the instability. The Laplace pressure is higher in the troughs than in the crests and thus the instability can develop.

In a series of papers [76] written between 1878 and 1892, Lord Rayleigh revisited and extended the work of Plateau. He showed that the instability of cylindrical films is established with a well-defined wavelength, and thus explained the regularity in spacing of the drops that form. The observed wavelength simply corresponds to the fastest growing mode and, for a thin film coating a fiber of radius b, being $2\pi\sqrt{2}b$, about $10\ b$.

For a polymeric solution which has higher molecular weight than usual liquids, the condition $S > S_c$ is satisfied. The polymer melt can spread over the interior of the pore walls. As stated earlier, when a liquid polymer is spreading on a solid high surface energy substrate, at microscopic spreading front the diffusion is realized by disentangled polymer chains, which suffer long-range forces, mainly van der Waals interactions. Because of the small value of the thickness of the precursor film, the wetting can be stabilized by the long-range van der Waals forces [77]. That means, for the wetting of high molecular weight polymer solutions, Rayleigh instability is suppressed after the generation of the very thin precursor films. If the wetting film has an intermediate thickness, linearly saturated instabilities occur. In the case of thick wetting films, Rayleigh instabilities grow corresponding to a certain extent to the mechanism found by Bernandiner [73].

2.5 Wetting of surfaces with critical mixtures

When wetting occurs with critical mixtures (i.e., mixtures what could be either mixed or decomposed on temperature T, pressure P or volume V), there is an interplay between wetting phenomena and the decomposition. In this context, critical point wetting and surface directed spinodal decomposition are discussed. These structure formation processes may be exploited to generate functional morphologies as in the case of platinum microtubes (c.f. Chapter 7).

2.5.1 Critical point wetting

In his paper [78], Cahn used only three equations and less than one column of text to show that if two phases, say fluid A and fluid B, approach a critical point in the presence of a non-critical phase C, then before the critical point is reached, one of the fluid phases completely wets the non-critical phase, and there is no contact between C and the other fluid phase. His argument was based on the thermodynamic stability condition, that the three surface energies obey the inequality:

$$|\gamma_{BC} - \gamma_{BC}| \leq \gamma_{AB} \tag{2.18}$$

He observed that the right hand side of this inequality vanished at the critical point as $(Tc-T)^{2\nu}$, where ν is the critical exponent, and he made the reasonable conjecture that the left hand side vanished as $(Tc-T)^3$. With the known values of the critical exponents $\nu \approx 0.65$, the inequality must become an equality before $(T_c - T)$ vanishes; hence a transition from non-wetting to wetting must occur as one approaches the critical point within the two-phase region of the phase diagram.

2.5.2 Surface-directed spinodal decomposition

Working with polymers has some benefits to unveil the spinodal phase decomposition, including the observation of the ripening of the phase structure and the time dependence of the size of individual domains. In the presence of a substrate, i.e., a non-critical matrix phase, this has been well exemplified by the surface-directed spinodal decomposition in polymer blends [79]. Spinodal decomposition, when occurring in the bulk, refers to spontaneous growth of concentration fluctuations with specific period [80]. This results in the generation of a near-ordered phase morphology on decomposition. The occurrence of halos on light scattering is caused by this near order. The halos represent the most frequent distance in the system. The period grows because of the ripening. The driving force for this is the reduction of the interface area between the co-existing phases. In the presence of viscous polymers, this Ostwald ripening process is so slow that it can be monitored with conventional methods. The system can be frozen by the solidification of the polymers at specific stages. This makes polymer extremely suitable to study the basic mechanism. The freezing at different stages also gives the possibility to generate specific morphologies required for corresponding applications.

However, in the presence of external surfaces, the separation process of the phases is directed by the external surface [81, 82]. In this process, phase separation dynamics does not proceed isotropically as it would in the bulk. Following the theoretical prediction by Ball and Essery [83], the first experimental observation of a "surface-directed spinodal decomposition" was reported by Jones and co-workers [79]. They studied spinodal decomposition of mixtures of poly(ethylenepropylene) (PEP) and perdeuterated poly(ethylenepropylene) (d-PEP) near the surface. Composition waves with wave vectors normal to, and which propagate inwards from, the surface have been found, which maintain coherence for several wavelengths. If the multicomponent system is confined, the phase morphology is strongly affected by substrate/film and film/air interfaces, as well as by confinement effects [84]. As a result, layered structure composition waves emanating from both interfaces interfere. The basic features of surface directed (micro-) phase separation in immiscible polymer systems have been presented in [79]. It was found that highly-ordered multilayered structures that extend over a large number of microdomains before a higher entropy state of disordered bulk domains occurs. The effect of finite film thickness on the kinetics of spinodal decomposition in a film thickness range where a transition from three-dimensional bulk-like to near two-dimensional kinetics was investigated by Sung *et al.* [85]. Below a certain threshold thickness, 2D phase structures where the domains penetrate through the whole film thickness, instead of layered structure, occur. Theoretical studies of the wetting behavior of two-phase systems confined inside cylindrical pores were proposed by Liu *el al.* [86]. Three configurations, respectively tubes, capsules, and plugs were proposed depending on the cylindrical pore radius, molecular length and temperature. It was also stated in the article that for small pores, there is a direct transition between plugs and the tube, while for larger pores there is an intermediate capsule regime. The formation of tubes and capsules correspond to the wetting while that of plugs to non-wetting.

2.6 Structure formation processes during the wetting of porous materials with polymeric liquids

2.6.1 Adaption of wetting phenomena from flat substrates to porous templates

Wetting phenomena described above are the key to template wetting for the preparation of 1D nano- and micro-objects. Organic polymers are among the materials with low surface energy [60, 87]. A polymeric melt or solution can be loaded with considerable proportions of low molar mass compounds. When a polymer-containing liquid is brought into contact with or a polymer melt is molten onto the surface of a porous membrane, wetting of the pore walls occurs while individual chains diffuse onto and along the pore walls as depicted in figure 2.7a. As a prerequisite, the pore walls must have a high surface energy. The processes discussed here are microscopic in nature, in contrast to phenomena such as the Lotus effect [88], which are associated with the macroscopic wettability of structured surfaces. Then, a mesoscopic precursor film will wet the walls of the pores in a similar manner to the formation of a precursor film on a flat substrate (figure 2.7b).

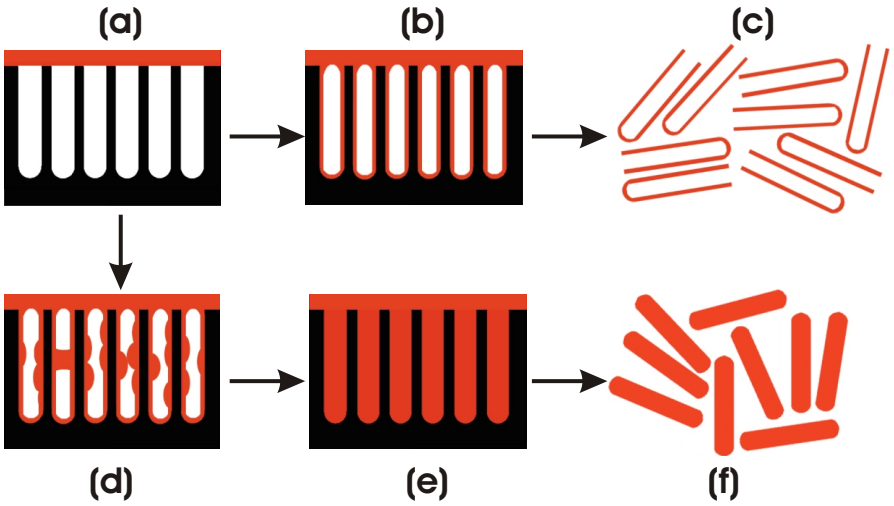

Figure 2.7: Wetting process of porous templates with polymer-containing liquids. (a) The fluid is brought into contact with the templates and covers the pore openings. (b) Within a certain time, the pore walls are covered by a mesoscopic film of the liquid. (c) Polymeric nanotubes obtained by selectively removing the template. (d) Formation of a meniscus in the case of wetting by nonpolymeric solutions. (e) Complete filling of pores. (f) Nanowires obtained by selectively removing the template.

In case of the spreading of liquids on flat substrates, the area to be wetted can be regarded as infinite and the liquid reservoir as finite. In case of pore wetting, however, the area to be wetted is finite, and the liquid reservoir infinite. If disordered liquids, for instance, molten homopolymers, are in contact with a porous material whose pore walls possess a sufficiently high surface energy (c.f. figure 2.7a), the wetting may occur as follows: at first, individual disentangled polymer chains diffuse on the pore wall. After a certain coverage has been reached, relaxation processes should occur. Both entropic relaxation (the polymer chains lying flat on the pore walls have an entropically unfavorable conformation), and the disjoining pressure that promotes a thickening of the wetting film could play a role. Typically, the walls of the thus-obtained tubes have a wall thickness of a few tens of nm, i.e., corresponding to the radii of gyration of typical polymers (c.f. figure 2.7b). This indicates that the tube walls consist of a

monolayer of macromolecules. The occurrence of Rayleigh instabilities (c.f. figure 2.7d), which is to be expected for liquid cylindrical films, is obviously suppressed. Eventually, the entire process may be frozen by the solidification of the polymeric layer. This can be accomplished by the evaporation of a solvent or thermal quenching, leading to vitrification or crystallization. Note that solid fibres are obtained if the diameter of the template pores is decreased below twice the wall thickness of the tubes.

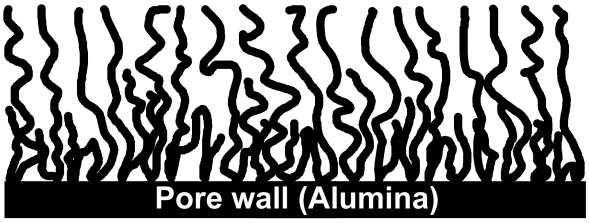

Figure 2.8: Absorption layer of polymer molecules on the inner pore walls of porous templates with a high surface energy. All the molecules are in direct contact with the pore walls, thus preventing the attractive interaction of the pore walls with another layer of the same material.

A point to note here is whether the final equilibrium state corresponds to a complete filling of the pore volume. If the diameters of the pores are much larger than the molecule size of the polymers, a complete filling (c.f. figure 2.7e) can only happen, if it occurs at all, at a completely different time scale, which is much longer than the time needed for wetting. This can be explained by the unusually large dimensions of the polymer molecules.

With polymer melts as well as polymer solutions the pore walls are completely wetted, with complete reproduction of the pore structure even for pore depths (T_p) of $100\ \mu m$. The liquid film solidifies when cooling or evaporation of the solvent leads to crystallization or vitrification. By selectively removing the templates, polymeric nanotubes (c.f. figure 2.7c) or nanowires (c.f. figure 2.7f) can be obtained .

Figure 2.9 depicts pore openings from the top of a macroporous silicon membrane that has been wetted by a homogeneous layer of PMMA-DR1 (poly(methyl methacrylate) with disperse red-1 side-chains). It is clear that the interior of the pore has not been filled completely, but only the pore walls coated by a polymeric layer homogeneously.

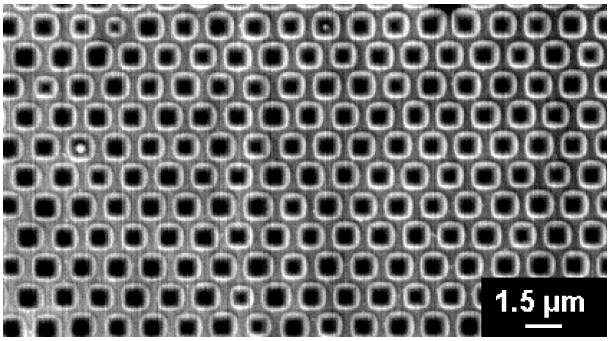

Figure 2.9: SEM image on the top of PMMA coated macroporous silicon. The pores are open with a visible layer of PMMA-DR1 which measures around 80 nm.

2.6.2 Occurrence of Rayleigh instabilities

The situation is very different in the case of template wetted by nonpolymeric liquids, in which the molecular weight as well as the size of the molecules is very low compared to that of polymers. As stated earlier, complete filling occurs in such systems thus leading to the formation of rods of low molar mass compounds. If a porous template is wetted by a nonpolymeric solution or an oligomeric solution, long-range intermolecular interactions lead to a wetting film consisting of many molecular layers on the pore walls as a result of the disjoining pressure. As

only a small fraction of the molecules is in direct contact with the pore walls, such multilayers are obviously more amenable to the occurrence of Rayleigh instabilities than macromolecular monolayers having the same thickness. This could lead to a formation of a meniscus, and is speculated to trigger the occurrence of Rayleigh instabilities described in section 2.4.3. This possibly leads to a complete filling of the pores after a certain time (c.f. figure 2.7d), similar to the mechanism observed by Bernadiner [73] (c.f. section 2.4.2.

In figure 2.10, the SEM pictures of PZT nanoshell tubes, which are obtained from an oligomeric precursor (figure 2.10a) and a mixture of the same oligomeric precursor with a polymer poly($_{D,L}$-lactide) (PDLLA) (figure 2.10b), are shown. The difference in the contrast corresponds to different wall thicknesses. It can be seen in figure 2.10a that the wall thickness is not homogeneous along the direction of the tube axis, but has an undulated morphology. This is because the precursor used is an oligomer with relatively low molar mass instead of a polymer with higher molecular weight. The wetting film on the pore walls consisting of the precursor-oligomer obviously had a thickness where linearly saturated Rayleigh instabilities occur (c.f. section 2.4.3). However, this undulation can be eliminated if a mixture of the oligomer and a polymer is used as the precursor. As shown in figure 2.10b, the wall thickness becomes homogeneous.

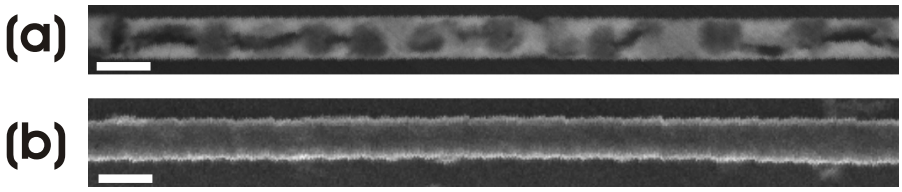

Figure 2.10: (a) Occurrence of Rayleigh instabilities within a PZT nanoshell tube wall along the tube axis due to the low molar mass precursor used (b) Rayleigh instability is suppressed after the low molar mass PZT precursor is mixed up with a polymer poly($_{D,L}$-lactide) (PDLLA). The scale bar in both images represents $1\ \mu m$.

2.6.3 Tailoring the morphology of the tube walls

A polymer in the form of a melt is placed on the porous templates at a temperature well above the glass transition point in the case of amorphous polymers, or well above the melting point in the case of partially crystalline polymers. The polymeric melt rapidly covers the pore walls. Alternatively, polymeric solutions may be dropped on the templates at ambient conditions.

As the pores are blind each with a capped end, the wetting layer has a tubular form which is an exact replica of the pore shape. A thermal treatment is usually necessary to get different target structures with desired materials and morphology:

- In case of oligomeric precursors contained in the tube walls to get inorganic ceramic tubular structures such as PZT or BTO nano(shell) tubes (c.f. Chapter 5), a first step of thermolysis at relatively low temperature at $300\,^{\circ}\mathrm{C}$ converts the oligomer into the target materials, but in an amorphous phase. Then, a second annealing step at higher temperature ($600^{\circ}\mathrm{C} \sim 850^{\circ}\mathrm{C}$) crystallizes the target materials within the tube walls into the perovskite phase.
- In case of pure polymeric melts such as the copolymer P(VDF-co-TrFE) (c.f. Chapter 6), which has the advantage that no pyrolysis is needed, thus avoiding the by-products during the process, porous templates wetted by a polymer are heated to a temperature above the

melting point in case of partially crystalline polymers. Then, cooling the sample to room temperature at specific cooling rates allows for a precise control of the crystallization process. The confined crystallization leads to the formation of specific textures of the tube walls.

- In case of organometallic precursors as used in the 3-component mixture $CHCl_3$/Pt(acac)$_2$/ PDLLA (c.f. Chapter 7), a first step of demixing by the evaporation of solvent ($CHCl_3$) leads to the coexistence of PDLLA-rich and Pt(acac)$_2$-rich phases (as described in figure 2.11a and figure 2.11b as well as in section 2.5.2). Then, a pyrolysis converts the Pt(II) into Pt(0). A final ripening process (as described in figure 2.11c) is needed to get closed Pt layers forming the tube walls whereas only distinct Pt particles are obtained without this process.

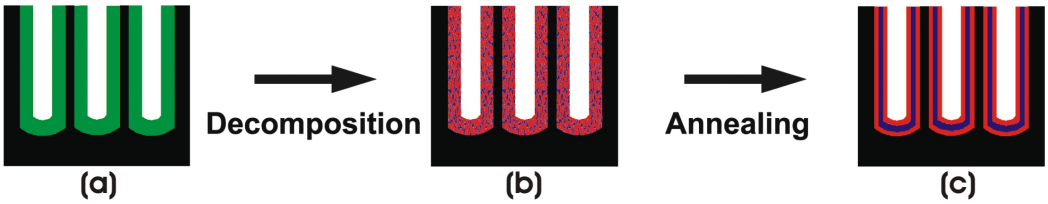

Figure 2.11: Formation of inorganic nanotubes within porous template via wetting by polymeric precursors: (a) formation of multi-component nanotubes; (b) decomposition by evaporation of solvent; (c) Ostwald ripening resulting in the growth of the crystallites of target materials with adjustable morphology sandwiched between two polymeric layers.

2.7 Summary of the chapter

In this chapter, wetting phenomena, which serve as a theoretical starting point for the rest of the thesis, are reviewed. First of all, wetting is described on a macroscopic scale. Important parameters such as spreading parameter and contact angle are explained in view of the Young's law. Then, on a microscopic scale, wetting is depicted by the existence of a thin precursor film as a result of the existence of long-range forces such as van der Waals interactions. Special features of polymers, such as variable chain lengths, small density fluctuations, and slow motions of long chains, open a new window on the classical wetting theory. Especially by wetting of polymers within confined geometry, new features can be obtained.

Then this general theory underlying wetting phenomena is adapted to a more specific case: wetting of porous templates, which entails the coexistence of polymer or polymeric solutions and a high surface energy pore walls, in order to fabricate functional 1D nano- and microstructures. This new approach is called *template wetting*. Important features such as structure formation, occurrence of Rayleigh instabilities, and tailoring of the morphology of the finally obtained tubes during the template-wetting process are described in details. A brief experimental procedure is sketched via phase separation and crystallization of targets materials within the polymeric matrix wetting the pore walls. Further detailed descriptions in the next chapters on the fabrication as well as characterization of 1D nano- and micro-objects with specific target materials are based on this chapter.